RESEARCH PAPER

Design, Synthesis, and Biological Evaluation of Luminescent Chalcone-based novel Pyridine derivatives Targeting DprE1 enzyme against H37Rv strain of Mycobacterium Tuberculosis.

Chilamakuri Nareshbabu[1], Chelluru Anusree[1], Kariyannagari Dhanunjay[1], Mallela Vijaya Jyothi[*2]

[1]*Department of Pharmaceutical Chemistry,Raghavendra Institute of Pharmaceutical Education and Research, Anantapuramu, Andhra Pradesh, India-515721*
[2]*Raghavendra Institute of Pharmaceutical Education and Research – Autonomous, K.R. Palli Cross, Chiyyedu, Anantapuramu, A.P. -51572.*
Email ID: drmvjyothiriper@gmail.com

ABSTRACT
Chalcones are versatile scaffolds in medicinal chemistry, owing to their reactive α,β-unsaturated carbonyl group and potential to form diverse nitrogen-containing heterocycles with significant pharmacological properties. In this study, thirty novel derivatives including indazolopyridines, cyanopyridines, and triazolopyridines—were synthesized from ten 2-acetylpyridine-based chalcones and evaluated for their anti-tubercular potential. The transformation of chalcones into these heterocycles involved nucleophilic cyclization followed by aromatization, exploiting the electrophilic β-carbon of the enone system. Molecular docking studies demonstrated favorable interactions with DprE1, a critical enzyme in Mycobacterium tuberculosis cell wall biosynthesis, indicating potential inhibitory efficacy. In silico ADME analysis confirmed drug-like properties, including high gastrointestinal absorption, solubility, and Lipinski compliance. Structural characterization was achieved through IR, ^{1}H NMR, ^{13}C NMR, and mass spectrometry. Luciferase reporter assay revealed potent antitubercular activity of several pyridine derivatives, notably I7, I8, P1, and C8, exhibiting over 95% inhibition against M. tuberculosis H37Rv. SAR analysis indicated that conjugated, donor–acceptor-rich scaffolds with strong luminescence also enhanced target affinity, suggesting promising theranostic potential..

Keywords: Chalcones; Anti-tubercular agent; Mycobacterium tuberculosis; DprE1; Molecular Docking.
How to cite this article: Nareshbabu C, Anusree C, Dhanunjay K, Jyothi MV; Design, Synthesis, and Biological Evaluation of Luminescent Chalcone-based novel Pyridine derivatives Targeting DprE1 enzyme against H37Rv strain of Mycobacterium Tuberculosis..Int J Drug Deliv Technol. . 2026;16(10s): 692-708; DOI: 10.25258/ijddt.16.10s.83
Source of support: Nil.
Conflict of interest: Nil

INTRODUCTION

According to the most recent WHO report on tuberculosis (TB) cases, TB has surpassed HIV/AIDS as the greatest infectious disease-related cause of death, indicating that it continues to pose an alarming situation to world health [1,2]. As per the recent studies, 1.25 million people died from tuberculosis in 2023 alone, and 10.8 million cases were reported globally (https://www.who.int/news-room/fact-sheets/detail/tuberculosis). Rather than a real increase in transmission, the backlog of undiagnosed cases and enhanced post-pandemic diagnostic skills are primarily responsible for the rise in TB incidence [3]. Among various strains of *Mycobacterium tuberculosis* (Mtb), extensively drug-resistant (XDR) and multidrug-resistant (MDR) strains significantly reduce the effectiveness of current treatment approaches [4,5]. Drug-sensitive TB (DS-TB) cases have responded well to the conventional first-line treatment, which consists of rifampicin (RIF), isoniazid (INH), pyrazinamide (PZA), and ethambutol (EMB).

However, chronic, XDR, and MDR TB cases are more complicated, and less proven and new medications like Bedaquiline (BDQ), fluoroquinolones, and linezolid are needed to treat MDR-TB and rifampicin-resistant TB (MDR/RR-TB). The development of completely drug-resistant TB (TDR-TB), which is resistant to every medication currently on the market, emphasizes the critical need for innovative treatment approaches. By rationally designing and developing novel anti-TB drugs with enhanced efficacy, decreased toxicity, and decreased resistance plays a crucial role in tackling these issues. Enzyme targeting drug discovery is an advanced approach which modulates the crucial activities of biological processes of Mycobacterium strains. DprE1 known as decaprenyl phosphoryl–β-d-ribose-2^{1}-epimerase, is a critical flavoenzyme in Mtb that plays a vital role in cell wall biosynthesis by catalyzing a key step in the production of arabinolactan and lipoarabinomannan. Inhibition of DprE1 enzyme may remain as a new strategy to discover novel antitubercular drugs.

Chalcones are naturally occurring bioactive compounds with various biological activities. Chalcones are necessary building blocks for the synthesis of semisynthetic and synthetic flavonoids and other heterocyclic compounds [6–8]. Chalcones have been found to possess potent antitubercular activity when they are cyclized. They have known to Inhibit InhA, a crucial enzyme in the fatty acid production pathway that produces mycolic acids [9,10]. Chalcones cause disruption of bacterial cell wall integrity which leads to death of Mycobacterium species.

**Author for Correspondence: drmvjyothiriper@gmail.com*

Indazolo pyridines derivatives of chalcones have shown a great deal of biological activity, such as antibacterial and antitubercular qualities, which makes them appealing candidates for additional medicinal chemistry research [11]. Because of their improved lipophilicity, bioavailability and binding affinities, cyanopyridines of chalcones are also a good choice for the development of anti-TB medications. The therapeutic potential of cyanopyridines has been further enhanced by hybrid compounds that combine them with different pharmacophores and exhibit synergistic effects. Triazole based compounds have drawn interest because of their resistance to enzymatic degradation and metabolic stability. 1,2,4-triazoles help to improve hydrogen bonding interactions with active site residues and increases potency, bioavailability and target binding. These substances interfere with the biosynthesis of bacterial cell wall and energy metabolism of Mycobacterium strains by inhibiting important mycobacterial enzymes such as ATP synthase, mycolic acid synthase, and enoyl-ACP reductase [12–14].

The present study emphasizes i*n silico* drug design, molecular docking with DprE1 and evaluation of anti TB activity against resistant strain of Mtb H37Rv of newly synthesized chalcones and their cyclized derivatives such as indazolo pyridines, cyanopyridines, and triazolopyridines.

Materials and Methods

ACD/ChemSketch software was used to draw the structures of the designed molecules. Molecular docking studies were performed using Schrödinger Glide software. Molecular properties such as log P, solubility, total polar surface area (TPSA), hydrogen bond acceptors (HBA), hydrogen bond donors (HBD), rotatable bonds (RB), Solubility (LogS), Lipinski rule violations, and synthetic accessibility were calculated using the SwissADME online drug design software. Melting points were determined using a capillary melting point apparatus. Infrared spectra (υ/cm) were recorded on a Bruker Alpha fourier-transform infrared spectroscopy. **^{1}H NMR** spectra were recorded in the specified solvent on a Bruker AMX 400 MHz spectrophotometer, with TMS as an internal standard. Mass spectra were obtained using a Hewlett-Packard 5988 spectrophotometer. All chemicals used in this study were procured from Sigma-Aldrich.

Virtual screening studies

Preparation of the macromolecule

The x-ray crystal structure of *Mycobacterium tuberculosis* DprE1 in complex with CT319 (PDB code: 4FDO), belongs to oxidoreductase classification with 2.40A° resolution obtained from *Mycobacterium tuberculosis*. This protein composed of chain A (oxidoreductase DprE1) with 481 amino acid residues without mutations, and co-crystal FAD, and 0T5 molecules. This protein imported into maestro workplace, pre-processed, optimized, and minimized by using the OPLS4 force field with default parameters [15].

Ligand preparation

The 2D chemical structures of molecules drawn in ACD/Chemsketch software and loaded into the Maestro workspace in *.MOL* format. Ligands underwent meticulous preparation for subsequent docking studies using Ligprep in Maestro. The Ligprep protocol involved energy minimization employing the OPLS_4 force field, with default settings applied for ionization states (considering possible states at the target pH of 7.0±2.0 using Epik), desalting, and retention of specified chiralities.

Molecular docking studies

The ligand docking Glide module was chosen from the Maestro tasks for conducting comprehensive docking studies of ligands [16,17]. Initially, the glide grid zip file and ligand outmaegz zip files were imported from the working directory. Subsequently, in the settings tab, the standard precision (SP) descriptor was selected to execute ligand docking, employing default parameters such as scaling of van der Waals radii (scaling factor: 0.80), partial charge cutoff (0.15), inclusion of Epik state penalties in the docking score, sampling of nitrogen inversions, sampling of ring conformations, and limiting the output to at most 1 pose per ligand (with a provision for up to 10 poses). The ligand docking outcomes were organized and indexed based on their interactions with amino acid residues within the binding pocket, with the ranking determined by the minimum binding energy to the maximum.

QSAR studies

QSAR is a mathematical relationship in the form of an equation between the biological activity and measurable physiochemical parameters [18]. QSAR's general mathematical form is represented by the following equation.

Biological Activity log (1/C) = f (Physicochemical Property)

To build a QSAR equation the following standard drugs IC_{50} values mentioned in the **Table 1** were taken and these IC_{50} values are converted into pIC_{50} by using the formula 6-LOG(IC_{50}). LogP, MR, TPSA, HBA, HBD, and RB physicochemical properties were used to build a QSAR equation. The various trials were tried by MLR model to get good QSAR equation by using BuildQSAR software.

Table 1. IC_{50}, pIC_{50}, and selected physicochemical descriptors of anti-tubercular drugs used for QSAR model development.

Name	IC50	pIC50	LogP	MR	TPSA	HBA	HBD	RB
Rifampin	1.9	5.721246	3.05	234.22	220.15	14	6	5
Ethambutol	57.6	4.239578	0.6	58.11	64.52	4	4	9

Rifabutin	35.4	4.450997	3.65	244.97	209.04	14	5	5
PAS	72.6	4.139063	0.43	39.83	83.55	3	3	1
Rifapentine	26.7	4.573489	4.06	251.34	220.15	14	6	6
Isoniazid	0.12	6.921	0.35	35.13	68.01	3	2	2

***In silico* ADME Studies**

In silico online data base Swiss ADME tool was used to get ADME properties like log P, molar refractivity, TPSA, HBA, HBD, RB, GI absorption, BBB permeability, log Kp, solubility, synthetic accessibility, etc. by providing synthesized molecular structures in SMILES notation.

General procedure for the synthesis of chalcones (C_1-C_{10})

Equimolar (0.005M) quantities of different aldehydes (3,4,5-trimethoxy benzaldehyde, 2-nitro benzaldehyde, pyridine-2-carbaldehyde, 2-methoxy benzaldehyde, 2-hydroxy-3-methoxy benzaldehyde, anthracene-9-carbaldehyde, naphthalene-2-carbaldehyde, piperazine-2-carbaldehyde, furan-2-carbaldehyde, and pyrrole-2-carbaldehyde) and 2-acetyl pyridine were taken in different tubes of parallel synthesizer (12 station). To this mixture in all tubes 1ml of methanol was added to ensure the solubility. Then 0.5ml of 10% KOH solution (not exceeding 0.001M) was added and stirred with a glass rod until it gets clear solution. The obtained mixture of all test tubes were tested for alkalinity and heated in parallel synthesizer for 2-3 hours at 60^0C. Then the solutions are cooled, the obtained mixtures were dried and recrystallized from ethanol. The completion of the reaction of all products were monitored by TLC by using ethyl acetate: n-hexane (7:3) as mobile phase [19,20].

General procedure for synthesis of indazolopyridines (I_1-I_{10})

0.0025M of chalcones (C^1-C_{10}) were taken in 10 parallel synthesizer tubes, 1-2 drops of acetone were added to all tubes to dissolve the chalcone, a mixture of 0.3265g of K_2CO_3 and 0.0025M of hydrazine hydrate was added then stirred to get a clear solution. Then this mixture was stirred about 1-2hrs at 50^0C. Then reaction mixtures were cooled then 0.002 M of ethyl acetoacetate was added to all tubes then stirred at room temperature about 1hr. The solid obtained cooled in ice cold water then purified by recrystallized from ethanol. Purity of the compounds was assessed by TLC using toluene and n-hexane (1:1) as mobile phasen [21,22].

General procedure for synthesis of triazolo pyridines (T_1-T_{10}):

An equimolar (0.0025M) mixture of chalcones (C_1-C_{10}) and sodium azide were taken in individual parallel synthesizer tubes. These mixtures were dissolved using 1-2 drops of methanol.0.0025 M of cupric oxide was added to all tubes as a catalyst then stirred well for 2-3 hrs. The obtained solids were dried and recrystallized from methanol. The completion of the reaction was monitored by TLC using ethyl acetate: *n*-hexane (1:1) as mobile phase [23,24].

General procedure for synthesis of cyanopyridines derivatives (P_1-P_{10}):

0.0025 M of chalcones (C_1-C_{10}) and 0.0025 M of malononitrile were taken in ten different parallel synthesizer tubes. To these tubes 0.0025 M of ammonium acetate was added and stirred well with a magnetic stirrer for about 3-4hrs. The obtained solids were dried and recrystallized with methanol. The completion of the reaction was monitored by TLC using toluene: n-hexane (6:4) as mobile phase [25].

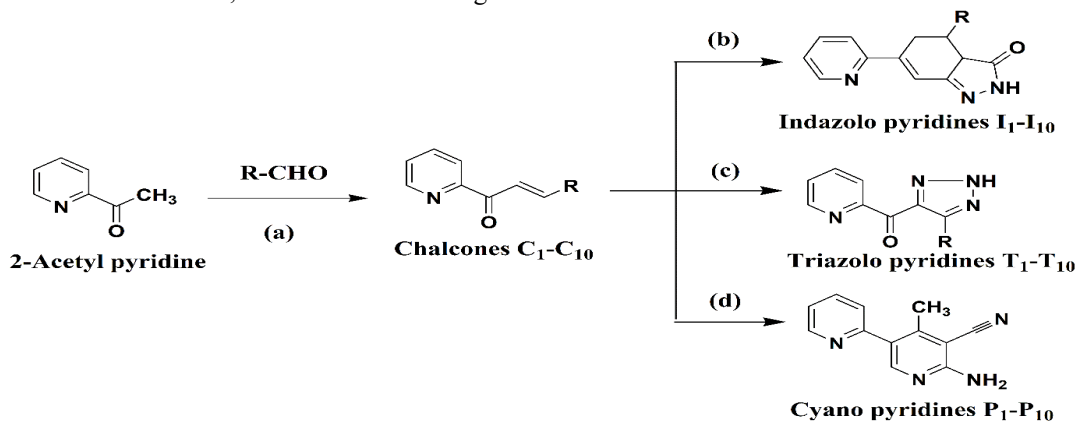

(a) MeOH, 10% KOH, 60^oC, 2-3hrs
(b) Acetone, Hydrazine hydrate, K_2CO_3, 50^oC, 1-2hrs
(c) Sodium azide, MeOH, CuO, 2-3hrs
(d) malanonitrile, CH_3COONH_4, 3-4hrs

R = 3,4,5-tri OCH_3 C_6H_2 for C_1, I_1, T_1, P_1; R = 2-NO_2 C_6H_4 for C_2, I_2, T_2, P_2; R = C_5H_4N for C_3, I_3, T_3, P_3; R = 2-OCH_3 C_6H_4 for C_4, I_4, T_4, P_4; R = 2-OH 3-OCH_3 C_6H_3 for C_5, I_5, T_5, P_5; R = $C_{14}H_9$ for C_6, I_6, T_6, P_6; R = $C_{10}H_7$ for C_7, I_7, T_7, P_7; R = $C_4H_5N_2$ for C_8, I_8, T_8, P_8;R = C_4H_3O for C_9, I_9, T_9, P_9; R = C_4H_4N for C_{10}, I_{10}, T_{10}, P_{10};

Antitubercular screening

Luciferase Reporter Phage (LRP) Assay

The Luciferase Reporter Phage test detects live Mtb by measuring bioluminescence generated from luciferase-expressing bacteriophages. Light emission occurs only in metabolically active cells, allowing differentiation between drug-sensitive (no light) and drug-resistant (light-producing) strains. In a modified LRP assay, synthesized indazoles, triazolo pyridines and cyanopyridines (100 µg/mL) were tested in G7H9 broth with *M. tuberculosis* H37Rv. DMSO (1%) was used as a control, and samples were incubated at 37°C for 72 hours. After adding $CaCl_2$ and mycobacteriophage phAETRC202, luminescence was measured as post-incubation with D-luciferin. The percentage RLU decrease was calculated, and compounds that reduced RLU by ≥50% were considered active against drug-resistant M. tuberculosis [26].

Results and Discussions

Molecular Docking studies

Docking score of the designed molecules with active site of the enzyme DprE1 which is essential for cell wall synthesis observed in screening by Schrodinger Glide software represented in Table 2. After protein preparation, the binding site was selected by making grid surrounding cocrystal 0T5. The resulting grid coordinates were determined as follows: X = 38.43, Y = 12.82, Z = 12.35, with grid dimensions of 30 A° x 30 A° x 30 A°. The structural quality of the 4FDO protein was evaluated using a Ramachandran plot to assess the backbone dihedral angles (φ and ψ) of its amino acid residues. As shown in Figure 1, the majority of residues were located in the most favored regions, indicating that the protein adopts a stable and stereo chemically reliable conformation. Only a small fraction of residues appeared in the additionally allowed or generously allowed regions, while very few, if any, were in disallowed regions. This distribution suggests that the 4FDO protein structure is geometrically sound and suitable for downstream computational analyses, such as molecular docking and molecular dynamics simulations. The high proportion of residues in the favored regions reflects proper folding and minimal steric clashes within the protein backbone, which is critical for maintaining the structural integrity of the active site and ensuring accurate predictions of ligand-binding interactions

.

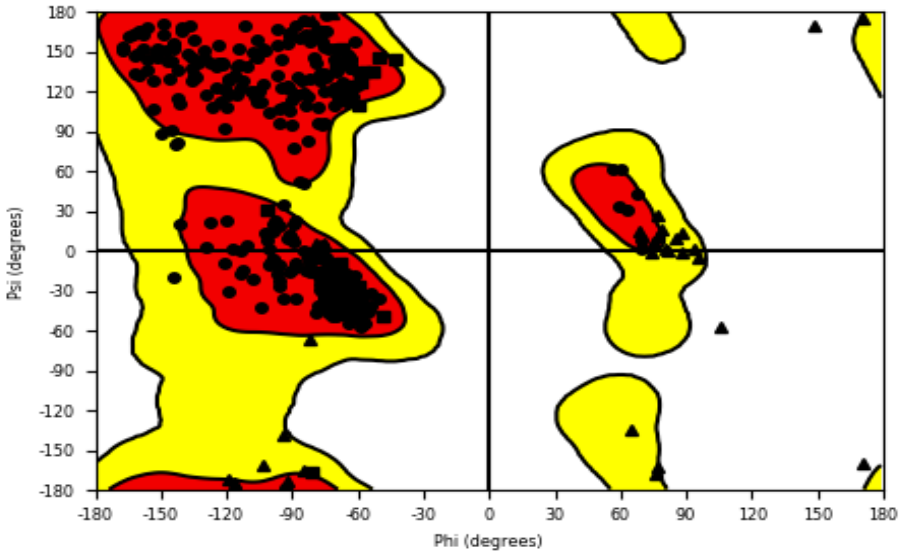

Figure 1. Ramachandran plot of the 4FDO protein structure showing the distribution of backbone dihedral angles (φ, ψ).

Table 2. Docking scores, Glide energies, and key binding interactions of compounds with the DprE1 enzyme.

Compound Code	**Docking score** ***(kcal/mol)***	**Glide energy** ***(kcal/mol)***	**Interactions**
Cocrystal_57339440	-8.04	-45.76	LYS418
I_5	-7.90	-50.37	HIS132, LYS418
I_1	-7.84	-53.56	HIS132, LYS418
C_8	-7.51	-39.74	ALA53
C_6	-7.45	-46.99	ASN385, LYS418
I_7	-7.42	-46.11	TYR60, HIS132, LYS418

I_6	-7.38	-48.29	ASN385, LYS418
I_4	-7.33	-44.49	TRP16, HIS132, LYS418
C_{10}	-7.29	-34.48	GLY55, GLY57
C_2	-7.25	-36.22	GLY117, ASN385
T_6	-7.24	-49.72	GLY117, HIS132, LYS418
C_1	-7.22	-45.87	LYS418
I_9	-7.17	-39.08	TYR415
I_{10}	-7.15	-39.04	TYR415, LYS418
C_5	-6.98	-40.40	ASN385, LYS418
C_3	-6.97	-35.15	LEU56
I_3	-6.93	-42.37	HIS132, TYR415, LYS418
T_{10}	-6.86	-41.48	HIS132, VAL365, ASN385, LYS418
I_2	-6.80	-45.22	TRP16, TYR60, GLY117, GLY321, LYS418
P_3	-6.70	-40.24	TYR60, LYS418
T_1	-6.69	-45.09	HIS132, LYS418
I_8	-6.66	-42.88	TRP16, TYR415, LYS418
P_9	-6.53	-39.01	TYR60, HIS132, LYS418
P_4	-6.48	-43.04	TRP16, TYR60, LYS418
C_4	-6.40	-36.46	ASN385, LYS418
P_{10}	-6.37	-39.22	TYR60, HIS132, LYS418
C_7	-6.33	-37.65	LYS418
P_2	-6.32	-43.28	LYS418
T_5	-6.16	-44.53	LEU317, LEU363, CYS387, LYS418
T_4	-6.11	-42.78	LEU317, LYS418
T_7	-6.10	-45.49	LEU317, LYS418
P_1	-6.07	-46.00	GLY117
T_2	-6.06	-41.94	HIS132, LYS418
C_9	-5.99	-29.98	ASN385
Isoniazid_3767	-5.80	-27.48	GLY55
T_3	-5.80	-40.00	TYR60, LEU317, LYS418
T_9	-5.61	-37.54	GLY117, HIS132
P_7	-5.59	-40.83	LYS418
P_8	-5.55	-39.58	HIS132, LYS418
P_5	-5.52	-43.42	LYS418
T_8	-5.27	-38.06	LEU317, LYS418
P_6	-3.93	-29.28	No interactions

The molecular docking analysis of various compounds against the DprE1 revealed several candidates with promising binding affinities when compared to the co-crystallized ligand (CID_57339440) and the standard drug isoniazid. The co-crystal ligand exhibited a docking score of -8.04 and Glide energy of -45.76, interacting with LYS418 a key residue frequently involved in binding across multiple compounds. Among the tested series, compounds I_5 (-7.90), I_1 (-7.84), and C_8 (-7.51) showed docking scores close to the co-crystal, with I_1 exhibiting the most favorable Glide energy (-53.56), indicating strong binding. These compounds frequently interacted with critical residues such as HIS132, LYS418, and ASN385, enhancing binding stability shown in Figure 2. In contrast, isoniazid showed the weakest docking score (-5.80) and Glide energy (-27.48), forming minimal interactions (only with GLY55), reflecting its limited affinity for this target site. Compounds from the "I" and "T" series consistently formed multiple interactions with catalytic residues like HIS132, TYR60, and TRP16, suggesting their potential as strong inhibitors. Notably, LYS418 emerged as a common interaction point,

reinforcing its relevance in ligand binding. Overall, many of the designed compounds, particularly from the I-series (e.g., I_1, I_5, I_7), surpassed the docking efficiency of both the co-crystal and isoniazid, highlighting their potential as promising leads for further antitubercular development. Overall, in molecular docking studies of indazoles, triazoles and cyanopyridines derivatives had indicated that indazoles have better binding score with DprE1enzyme.

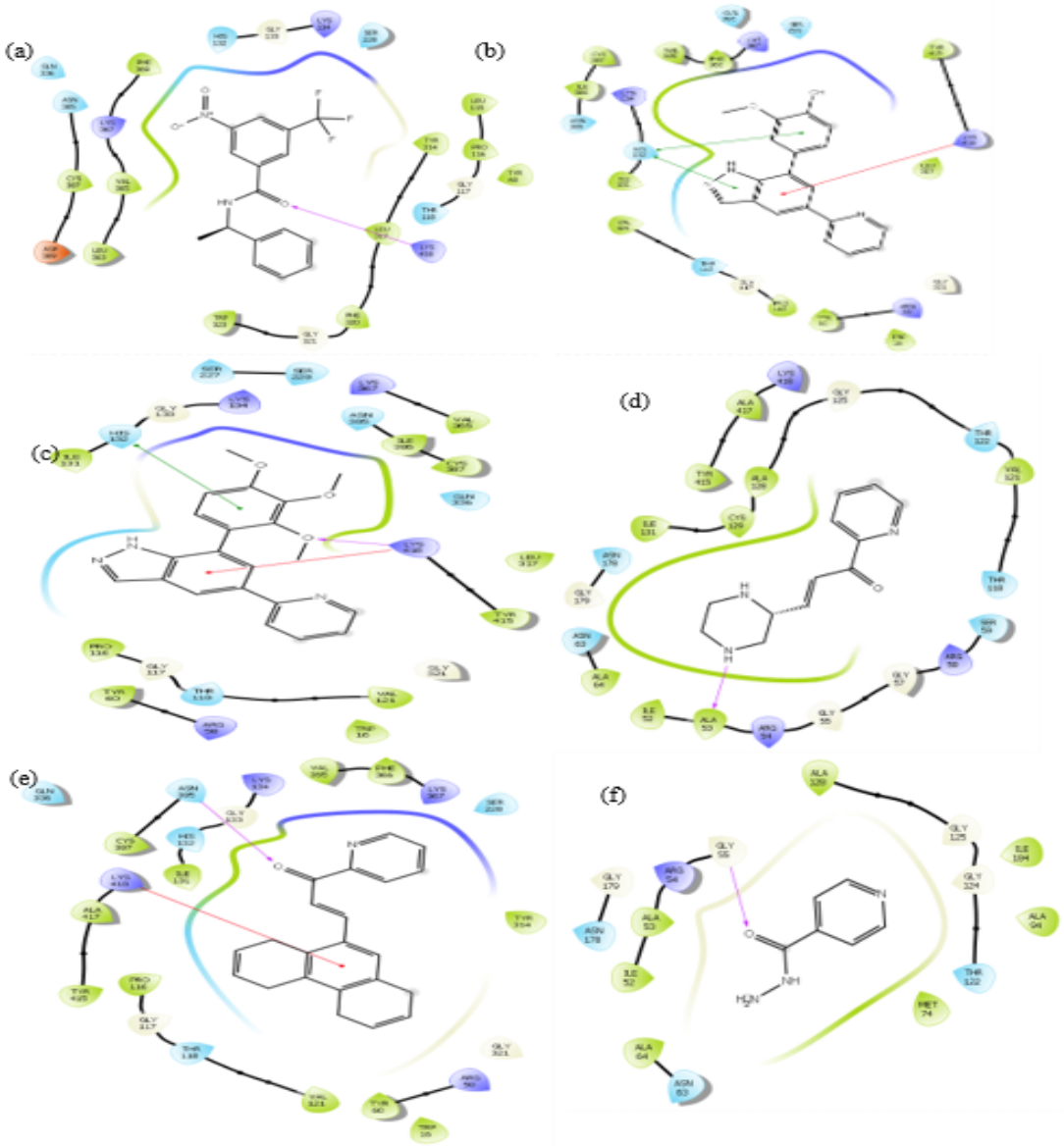

Figure 2. Docking interactions of ligands with the DprE1 enzyme: (a) co-crystal ligand (CID: 57339440), (b) I5, (c) I1, (d) C8, (e) C6, and (f) Isoniazid.

QSAR studies

The descriptors LogP, MR, and HBA among the selected descriptors exhibited high R^2 value (0.910) in correlation with biological activity of the standards mentioned in Table 2 and the following QSAR equation was identified. Y1 = + 8.6028 (± 10.8160) X1 - 0.5834 (± 0.6125) X2 + 8.3557 (± 8.4565) X4 - 0.8443 (± 6.1328). The above equation obtained is utilized to calculate the pIC50 values of the designed compounds represented in Table 3. Correlation analysis by MLR model of the above generated QSAR equation showed in Figure 3.

Table 3. Predicted biological activity data of the selected compounds using the MLR model.

Compound Code	pIC_{50}	Compound Code	pIC_{50}	Compound Code	pIC_{50}	Compound Code	pIC_{50}
C_1	14.043	I_1	3.6062	T_1	22.091	P_1	11.237
C_2	7.787	I_2	-5.326	T_2	13.152	P_2	16.235
C_3	5.781	I_3	-4.586	T_3	7.2748	P_3	6.056
C_4	6.383	I_4	-8.537	T_4	13.813	P_4	10.959
C_5	12.442	I_5	-1.710	T_5	14.452	P_5	6.781
C_6	-16.42	I_6	-27.02	T_6	-14.88	P_6	8.762
C_7	-5.837	I_7	-22.72	T_7	-7.417	P_7	8.310
C_8	5.305	I_8	-4.545	T_8	10.234	P_8	3.773
C_9	6.082	I_9	-4.371	T_9	11.447	P_9	13.927
C_{10}	-6.927	I_{10}	-17.72	T_{10}	6.6039	P_{10}	7.349

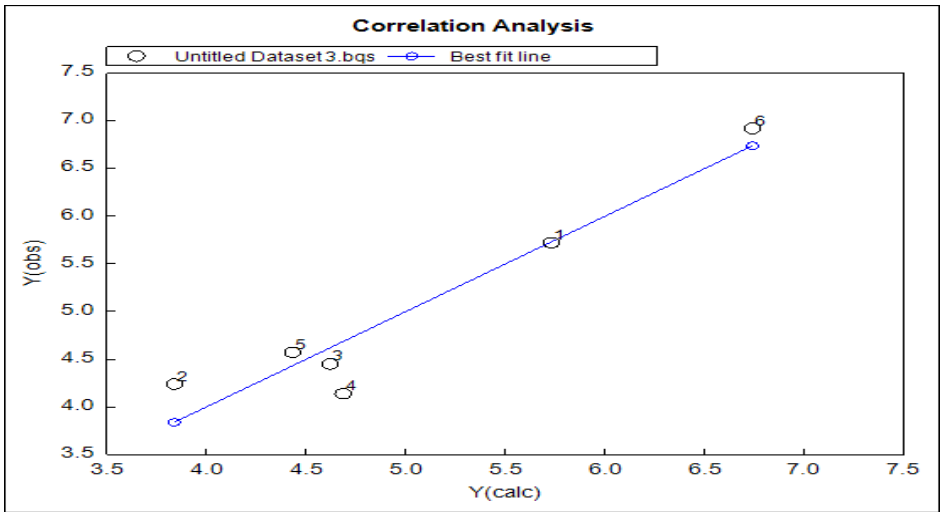

Figure 3. Correlation plot between observed and calculated biological activities of the standard compounds.

The designed molecules demonstrated significantly enhanced predicted biological activity compared to standard anti-tubercular drugs. Notably, compounds T1 (pIC_{50} = 22.091), P2 (pIC_{50} = 16.235), C1 (pIC_{50} = 14.043), T5 (pIC_{50} = 14.452), T4 (pIC_{50} = 13.813), and P9 (pIC_{50} = 13.927) exhibited exceptionally high predicted potency, with pIC_{50} values far exceeding that of Isoniazid, the most potent standard drug (pIC_{50} = 6.921). In addition, moderately active compounds such as P1 (pIC_{50} = 11.237), T2 (pIC_{50} = 13.152), and P4 (pIC_{50} = 10.959) also

demonstrated superior predicted activity compared to conventional treatments, making them promising candidates for further investigation. However, some molecules, including C6, I6, T6, and I7, showed negative

pIC_{50} values, indicating poor or negligible predicted biological activity and thus are not suitable for further development. Overall, the majority of the designed molecules exhibited higher predicted potency than standard drugs, suggesting their potential for greater therapeutic efficacy.

ADME studies

Swiss ADME studies of all the synthesized compounds *viz.*, chalcones, indazoles, triazoles and cyanopyridines (C_1-C_{10}, I_1-I_{10}, T_1-T_{10} and P_1-P_{10}) shown in Table 4 [27]. The ADME profiling of the designed compounds reveals favorable drug-like properties across the majority of the series. Most compounds exhibit acceptable molecular weights (ranging between ~110–450 Da) and Log P values within drug-like ranges, suggesting good membrane permeability and bioavailability. All compounds comply with Lipinski's Rule of Five, indicating a lower likelihood of oral bioavailability issues. High gastrointestinal (GI) absorption was predicted for all compounds, with several also showing blood–brain barrier (BBB) permeability, particularly among the "I" and "C" series molecules. Solubility varied across the series: many compounds were categorized as moderately or poorly soluble based on Log S values, though a few, notably T8, C8, and C9, were classified as soluble, which is favorable for oral formulations. Importantly, all designed molecules demonstrated reasonable synthetic accessibility scores (ranging from 2.4–3.4), indicating they can be synthesized without significant synthetic challenges. Overall, the ADME profiles suggest that the majority of the designed compounds possess promising drug-like characteristics, warranting further optimization focusing particularly on improving solubility for a few candidates.

Table 4. Predicted ADME properties of the screened compounds obtained from *SwissADME*.

Compound Code	Mol. Wt	Log P	Molar refractivity	TPSA	HBA	HBD	RB	GI absorption & BBB permeant	Log S	Solubility Class	Lipinski's rule of 5	Synthetic accessibility
P_1	362.38	2.46	101.50	103.28	6	1	5	High & No	-6.75	Poorly soluble	Yes	3.27
P_2	317.31	3.29	90.85	121.41	5	1	3	High & No	-5.78	Moderately soluble	Yes	2.85
P_3	273.30	2.33	79.82	88.48	4	1	2	High & No	-6.04	Poorly soluble	Yes	2.78
P_4	302.33	3.49	88.52	84.82	4	1	3	High & No	-6.53	Poorly soluble	Yes	2.76
P_5	318.33	2.17	90.54	105.05	5	2	3	High & No	-5.95	Moderately soluble	Yes	2.88
P_6	450.53	6.14	117.04	75.59	3	1	2	High & No	-9.71	Poorly soluble	Yes	3.15
P_7	322.36	4.90	99.53	75.59	3	1	2	High & No	-8.07	Poorly soluble	Yes	2.93
P_8	280.34	1.60	87.29	99.65	5	3	2	High & No	-4.88	Moderately soluble	Yes	3.35
P_9	262.27	2.87	74.29	88.73	4	1	2	High & No	-5.63	Moderately soluble	Yes	3.09
P_{10}	261.29	2.46	79.52	87.62	4	2	2	High & No	-4.83	Moderately soluble	Yes	3.20
I_1	361.29	2.73	104.24	69.26	5	1	5	High & Yes	-7.91	Poorly soluble	Yes	3.10

I_2	288.30	1.94	93.58	87.39	4	1	3	High & No	-6.93	Poorly soluble	Yes	2.61
I_3	236.28	2.25	82.56	54.46	3	1	2	High & Yes	-7.20	Poorly soluble	Yes	2.48
I_4	333.34	2.38	91.25	50.80	3	1	3	High & Yes	-7.69	Poorly soluble	Yes	2.53
I_5	317.34	2.34	93.28	71.03	4	2	3	High & Yes	-7.11	Poorly soluble	Yes	2.64
I_6	373.44	3.10	119.23	41.57	2	1	2	High & Yes	-9.83	Poorly soluble	Yes	3.40
I_7	323.39	2.45	102.27	41.57	2	1	2	High & Yes	-9.23	Poorly soluble	Yes	2.64
I_8	141.18	1.79	90.03	65.63	4	3	2	High & No	-6.04	Poorly soluble	Yes	2.99
I_9	110.16	1.90	77.03	54.71	3	1	2	High & Yes	-6.79	Poorly soluble	Yes	2.84
I_{10}	140.20	1.46	79.11	53.36	2	2	2	High & Yes	-6.79	Poorly soluble	Yes	2.46
T_1	276.29	1.90	88.96	99.22	7	1	6	High & No	-3.44	Moderately soluble	Yes	3.17
T_2	260.24	1.11	78.31	117.35	6	1	4	High & No	-3.30	Moderately soluble	Yes	2.70
T_3	251.25	0.65	67.28	84.42	5	1	3	High & No	-2.64	Moderately soluble	Yes	2.83
T_4	296.33	2.00	75.98	80.76	5	1	4	High & No	-3.32	Moderately soluble	Yes	2.67
T_5	296.29	1.24	78.00	100.99	6	2	4	High & No	-3.63	Moderately soluble	Yes	2.78
T_6	350.37	1.57	104.50	71.53	4	1	3	High & Yes	-5.34	Poorly soluble	Yes	3.02
T_7	322.32	1.25	86.99	71.53	4	1	3	High & Yes	-4.40	Poorly soluble	Yes	2.81
T_8	258.29	0.53	74.76	95.59	6	3	3	High & No	-1.29	soluble	Yes	3.15
T_9	240.22	0.76	61.75	84.67	5	1	3	High & No	-2.65	Moderately soluble	Yes	2.81
T_{10}	239.24	1.31	63.84	87.32	4	2	3	High & No	-2.48	Moderately soluble	Yes	2.81

C_1	313.42	2.81	87.53	57.65	5	0	7	High & Yes	-3.70	Moderately soluble	Yes	2.63
C_2	254.24	2.06	72.87	75.78	4	0	4	High & Yes	-3.37	soluble	Yes	2.77
C_3	210.23	2.05	61.84	42.85	3	0	3	High & Yes	-2.71	Moderately soluble	Yes	2.61
C_4	239.26	2.71	70.54	39.19	3	0	4	High & Yes	-3.66	Moderately soluble	Yes	2.51
C_5	255.26	2.58	72.56	59.42	4	1	4	High & Yes	-3.25	Moderately soluble	Yes	2.58
C_6	313.38	2.89	97.96	29.96	2	0	3	High & Yes	-5.18	Moderately soluble	Yes	3.25
C_7	259.29	2.97	81.00	29.96	2	0	3	High & Yes	-4.25	Moderately soluble	Yes	2.94
C_8	217.27	1.53	69.31	54.02	4	2	3	High & No	-1.32	soluble	Yes	3.00
C_9	199.20	1.71	56.31	56.31	3	0	3	High & Yes	-2.71	soluble	Yes	2.61
C_{10}	198.22	1.31	58.39	45.75	2	1	3	High & Yes	-3.79	soluble	Yes	2.58

Chemistry

The synthesized compounds (**C_1-C_{10}**) in step 1 are sterically (E) isomers with α, β-unsaturated carbonyl moiety and characterized as 1,3-diaryl-2-propen-1-ones. These compounds possess electrophilic reactive moieties attached to C=C-C=O system and facilitated the synthesis of heterocyclic derivatives such as indazoles, triazoles and cyanopyridines compounds through 1, 2-addition at carbonyl group or 1,4-conjugate addition and cyclization.

1-pyridin-2-yl-4-(3,4,5-trimethoxyphenyl)but-2-en-1-one (C_1)
Formula $C_{20}H_{18}N_4O_3$, Yield: 82%, m.p. 290°C, R_f value 0.72; IR (KBr, $V_{max,}$ cm^{-1}): 3055.45 (C-H), 1580.21 (C=C), 1598.12 (C=N) pyridine ring, 1720.31 (C=O), 1654.91 (αC=C), 3060.38 (CH), 1554.36 (C=C benzene ring), 3022.44 (C-H), 1250.14 (C-O Methoxy group); ^{1}H NMR (500 MH_Z, $CDCl_3$) δ 2.95 (m, 2H, -CH_2), 3.69 (9H, S, -OCH_3 groups), 6.12, 7.35 (t, 1H, -CH=), 6.35-6.54 (m, 2H, aromatic), 7.55-9.09 (4H, d(2), t(2) Pyridine ring); MS m/z 313.347.

3-(2-nitrophenyl)-1-pyridin-2-ylprop-2-en-1-one (C_2)
Formula $C_{17}H_{11}N_5O_2$, Yield 79%, m.p 276°C, R_f value 0.79; IR (KBr,$V_{max,}$$cm^{-1}$): 3050.63 (C-H), 1545.39 (C=C), 1587.34 (C=N) pyridine ring, 1720.64 (C=O), 1465.74 (α C=C), 3065.59 (C-H), 1560.63 (C=C benzene ring), 1350.71 (C-N nitro group); ^{1}H NMR (500 MH_Z, $CDCl_3$) δ 6.65-6.85 (2H, d(2) prop-2-ene-1-one bridge), 7.35-9.10 (8H, m, benzene and pyridine ring); MS m/z 254.2408.

1,3-dipyridin-2-ylprop-2-en-1-one (C_3)
Formula $C_{16}H_{11}N_5$, Yield 81%, m.p 256°C, R_f value 0.76; IR (KBr, V_{max}, Cm^{-1}) 3087.69 (C-H), 1566.89 (C=C), 1612.42 (C=N) pyridine ring, 1722.81 (C=O), 1633.13 (α C=C), 3088.47 (C-H), 1567.53 (C=C), 1480.50 (C=N) pyridine ring; ^{1}H NMR (500 MH_Z, $CDCl_3$) δ 7.22-7.49 (2H, d(2) prop-2-ene-1-one bridge), 7.65-9.05 (8H, m, pyridine ring); MS m\z 210.2313.

3-(2-methoxyphenyl)-1-pyridin-2-ylprop-2-en-1-one (C_4)
Formula $C_{18}H_{14}N_4O$, Yield: 79%, m.p 267°C, R_f value 0.74; IR (KBr, V_{max}, Cm^{-1}): 3096.48 (C-H), 1569.54 (C=C), 1615.15 (C=N) pyridine ring, 1719.49 (C=O), 1623.10 (α C=C), 3065.67 (C-H), 1542.69 (C=C benzene ring) 2840.51 (C-H), 1250.91 (C-O methoxy group); ^{1}H NMR (500 MH_Z, $CDCl_3$) δ 3.55 (3H, 1S, -OCH_3), 6.48-6.63 (2H, d(2) and prop-2-ene-1-one bridge), 6.95-8.95 (8H, m, benzene and pyridine); MS m\z 239.39236.

3-(2-hydroxy-3-methoxyphenyl)-1-pyridin-2-ylprop-2-en-1-one (C_5):
Formula $C_{15}H_{13}NO_3$, Yield 83%, m.p 285°C, R_f value 0.85; IR (KBr, V_{max}, Cm^{-1}): 3077.39 (C-H), 1553.29 (C=C), 1616.61 (C=N Pyridine), 1580.45 (C=C), 1480.91 (C=N) pyridine ring, 1708.62 (C=O), 1646.72 (α C=C), 3087.69

(C-H), 1542.31 (C=C benzene ring), 3500.58 (O-H), 2835.81 (C-H), 1250.91 (C-O); ^{1}H NMR (500 MHz, $CDCl_3$) δ 3.24 (3H, S, -OCH_3), 5.15 (1H, S, -OH), 6.22-6.45 (2H, d(2) prop-2-1-one bridge), 6.81-8.75 (7H, m, pyridine, and aromatic); MS m\z 255.26862.

1-pyridin-2-yl-3-(1,4,5,8-tetrahydrophenanthren-9-yl)prop-2-en-1-one (C_6)
Formula $C_{22}H_{15}NO$, Yield 85%, m.p 286°C, R_f value 0.84; IR (KBr, V_{max}, Cm^{-1}): 3064.17 (C-H), 1546.75 (C=C), 1602.19 (C=N) pyridine ring 1707.96 (C=O), 1623.46 (α C=C), 3025.36 (C-H), 1590.16 (C=C phenanthrene ring); ^{1}H NMR (500 MHz, $CDCl_3$) δ 6.47-6.84 (2H, d(2) prop-2-ene-1-one bridge), 7.45-8.83 (12H, m, phenanthrene and pyridine ring); MS m/z 309.36.

3-naphthalen-1-yl-1-pyridin-2-ylprop-2-en-1-one (C_7)
Formula $C_{18}H_{13}NO$, Yield 87%, m.p 285°C, R_f value 0.85; IR (KBr, V_{max}, Cm^{-1}): 3058.29 (C-H), 1535.57 (C=C), 1607.48 (C=N) pyridine ring, 1722.47 (C=O), 1643.56(α C=C), 3046.36 (C-H), 1600.42 (C=C naphthalene ring); ^{1}H NMR (500 MHz, $CDCl_3$) δ 6.62-6.70 (2H, d(2) prop-2-ene-1-one bridge), 7.05-8.76 (10H, m, naphthalene and pyridine ring); MS m/z 259.30192.

3-piperazin-2-yl-1-pyridin-2-ylprop-2-en-1-one (C_8)
Formula $C_{12}H_{15}N_3O$, Yield 85%, m.p 286°C, R_f value 0.86; IR (KBr, V_{max}, Cm^{-1}): 3085.53 (C-H), 1567.46(C=C), 1537.58 (C=N) pyridine ring, 1704.58 (C=O), 1632.36 (α C=C), 3200.57 (N-H), 3049.46 (C-H), 1200.24 (C-N piperazine ring); ^{1}H NMR (500 MHz, $CDCl_3$) δ 2.51-3.59 (7H, d(3), t(3), m(1) piperazine), 6.19-6.78 (2H, d(2) prop-2-ene-1-one bridge), 7.65-8.33 (4H, d(2), t(2) pyridine ring); MS m/z 217.267.

3-furan-2-yl-1-pyridin-2-ylprop-2-en-1-one (C_9)
Formula $C_{12}H_9NO_2$, Yield 86%, m.p 285°C, R_f value 0.84; IR (KBr, V_{max}, Cm^{-1}): 3091.31 (C-H), 1574.58 (C=C), 1614.14(C=N) pyridine ring, 1719.96 (C=O), 1632.54 (α C=C), 3100.61 (C-H), 1564.32 (C=C), 1200.74 (C-O furan ring); ^{1}H NMR (500 MHz, $CDCl_3$) δ 76.62-6.75 (2H, d(2) prop-2-ene-1-one bridge), 7.05-9.02 (7H, m, oxole, and pyridine ring); MS m/z 199.205

1-pyridin-2-yl-3-(1*H*-pyrrol-2-yl)prop-2-en-1-one (C_{10})
Formula $C_{12}H_{10}N_2O$, Yield 85%, m.p 286°C, R_f value 0.86; IR (KBr, V_{max}, Cm^{-1}): 3073.38 (C-H), 1544.86 (C=C), 1567.45(C=N) pyridine ring, 1714.45 (C=O), 1643.27 (α C=C), 3350.57 (N-H), 1553.57 (C=C), 1300.57 (C-N pyridine ring); ^{1}H NMR (500 MHz, $CDCl_3$) δ 5.72-6.36 (3H, d(2), t(1) and azole ring), 6.65-691 (2H, t(1), m(1) but-2-ene-one bridge), 7.72-8.35 (4H, d(2), t(2) pyridine ring),; MS m/z 198.220

5-pyridin-2-yl-7-(2,3,4-trimethoxyphenyl)-1*H*-indazole (I_1)
Formula $C_{21}H_{19}N_3O_3$, Yield 86%, m.p 284°C, R_f value 0.85; IR (KBr, V_{max}, Cm^{-1}): 3065.73 (C-H), 1532.67 (C=C), 1578.56 (C=N) pyridine ring, 3397.37 (N-H), 3100.58 (C-H), 1553.57 (C=C), 1590.36 (C-N indazole ring), 3000.46 (C-H), 2840.16 (C-H), 1550.85 (C=C), 1250.35 (C-O), 1450.57 (C-H trimethoxy benzene); ^{1}H NMR (500 MHz, $CDCl_3$) δ 3.73 (9H, S, -OCH_3), 6.18-8.66 (9H, m, pyridine and aromatic rings), 12.22 (1H, d, -NH of indazole); MS m/z 361.398.

7-(4-nitrophenyl)-5-pyridin-2-yl-1*H*-indazole (I_2)
Formula $C_{18}H_{12}N_4O_2$, Yield 85%, m.p 285°C, R_f value 0.86; IR (KBr, V_{max}, Cm^{-1}): 3087.90 (C-H), 1554.64 (C=C), 1564.79 (C=N), 1350.24 pyridine ring, 3368.58 (N-H), 3100.13 (C-H), 1600.68 (C=C), 1350.58 (C-N indazole ring), 3050.47 (C-H), 1570.36 (C=C), 1300.57 (C-N nitro benzene); ^{1}H NMR (500 MHz, $CDCl_3$) δ 7.45-8.65 (11H, d, t, m pyridine and aromatic ring), 11.88 (1H, d, -NH of indazole ring); MS m/z 316.313

5,7-dipyridin-2-yl-1*H*-indazole (I_3)
Formula $C_{17}H_{12}N_4$, Yield 86%, m.p 286°C, R_f value 0.85; IR (KBr, V_{max}, Cm^{-1}): 3015.68 (C-H), 1532.59 (C=C), 1587.46 (C=N), 1543.57 pyridine ring, 3256.58 (N-H), 3100.24 (C-H), 1600.57 (C=C), 1350.58 (C-N indazole ring), 3000.85 (C-H), 1590.96 (C=C) 1480.53 (C=N pyridine ring); ^{1}H NMR (500 MHz, $CDCl_3$) δ 7.25-8.60 (11H, d, t, m, pyridine and aromatic ring), 12.02 (1H, s, -NH of indazole); MS m/z 272.303

7-(4-methoxyphenyl)-5-pyridin-2-yl-1*H*-indazole (I_4)
Formula $C_{19}H_{15}N_3O$, Yield 85%, m.p 285°C, R_f value 0.86; IR (KBr, V_{max}, Cm^{-1}): 3062.35 (C-H), 1521.24 (C=C), 1597.57 (C=N), 1350.47 pyridine ring, 3369.25 (N-H), 3100.36 (C-H), 1643.26 (C=C), 1350.96 (C-N indazole ring), 3062.63 (C-H), 2840.37 (C-H), 1596.26 (C=C), 1250.48 (C-O), 1450.34 (C-H methoxy benzene); ^{1}H NMR (500 MHz, $CDCl_3$) δ 3.29 (3H, S, -OCH_3), 6.38-8.60 (11H, d, t, m pyridine and aromatic ring), 11.67 (1H, d, -NH of indazole); MS m/z 301.341

2-methoxy-4-(5-pyridin-2-yl-1*H*-indazol-7-yl)phenol (I_5)
Formula $C_{19}H_{15}N_8O_3$, Yield :85%, m.p 285°C, R_f value 0.86; IR (KBr, V_{max}, Cm^{-1}): 3020.57 (C-H), 1462.58 (C=C), 1596.32 (C=N), 1350.75 pyridine ring , 1593.75 (N-H), 3032.87 (C-H), 1532.86(C=C), 1350.54 (C-N indazole ring), 3073.24 (C-H), 2840.57 (C-H), 1550.36 (C=C), 1250.58 (C-O), 1450.25 (C-H methoxy benzene); ^{1}H NMR (500 MHz, $CDCl_3$) δ 3.55 (3H, S, -OCH_3), 5.14 (1H, S, -OH), 6.86-8.58 (10H, d, t, m pyridine ring and aromatic ring), 12.9 (1H, d, -NH of indazole ring); MS m/z 317.341

7-(anthracen-10-yl)-5-(pyridin-2-yl)-1H-indazole (I_6)
Formula $C_{26}H_{17}N_3$, Yield 86%, m.p 284°C, R_f value 0.85; IR (KBr, V_{max}, Cm^{-1}): 3052.75 (C-H), 1495.47 (C=C), 1589.25 (C=N), 1350.24 pyridine ring, 1594.85 (N-H), 3124.36 (C-H), 1657.87 (C=C), 1350.56 (C-N indazole ring), 3100.32 (C-H), 1620.76 (C=C phenanthrene ring); ^{1}H NMR (500 MHz, $CDCl_3$) δ 7.05-8.39 (16H d, t, m pyridine and anthracene ring), 12.13 (1H, d, -NH of indazole ring); MS m/z 371.43

7-naphthalen-1-yl-5-pyridin-2-yl-1*H*-indazole (I_7)

Formula $C_{22}H_{15}N_3$, Yield 84%, m.p 286°C, R_f value 0.86; IR (KBr, V_{max}, Cm^{-1}): 3025.65 (C-H), 1571.54 (C=C), 1582.45 (C=N)pyridine ring,3356.24 (N-H), 3132.35 (C-H), 1642.59 (C=C), 1350.32 (C-N indazole ring), 3132.83 (C-H), 1620.62 (C=C naphthalene ring); ^{1}H NMR (500 MH_Z, $CDCl_3$) δ 6.90-8.62 (14H, d, t, m pyridine and naphthalene ring), 12.11 (1H, d, -NH of indazole ring); MS m/z 321.374

7-piperazin-2-yl-5-pyridin-2-yl-1*H*-indazole (I_8)
Formula $C_{16}H_{15}N_3$, Yield 86%, m.p 285°C, R_f value 0.85; IR (KBr, V_{max}, Cm^{-1}): 3056.38 (C-H), 1567.58(C=C), 1562.70 (C=N)pyridine ring, 3345.76 (N-H), 3125.46 (C-H), 1679.76 (C=C), 1350.28 (C-N indazole ring), 3300.59 (N-H), 2900.45 (C-H), 1200.73 (C-N piperazine ring); ^{1}H NMR (500 MH_Z, $CDCl_3$) δ 2.0-4.14 (9H, m, piperazine ring), 6.96-8.63 (7H, d, t, m pyridine and aromatic ring) 12.60 (1H, d, -NH of indazole ring); MS m/z 279.339

7-furan-2-yl-5-pyridin-2-yl-1*H*-indazole (I_9)
Formula $C_{16}H_{11}N_3O$, Yield 84%, m.p 284°C, R_f value 0.84; IR (KBr, V_{max}, Cm^{-1}): 3092.89 (C-H), 1489.77 (C=C), 1602.85 (C=N), 1350.67pyridine ring, 1569.17 (N-H), 3139.25 (C-H), 16 (C=C), 1350.27 (C-N indazole ring), 1693.76 (C=C), 1220.36 (C-O furan ring); ^{1}H NMR (500 MH_Z, $CDCl_3$) δ 6.22-6.49 (3H, d(2), t(1) furan ring), 7.08-8.68 (7H, d, t, m pyridine and aromatic ring), 11.74 (1H, S, -NH of indazole ring); MS m/z 261.278

5-pyridin-2-yl-7-(1*H*-pyrrol-2-yl)-1*H*-indazole (I_{10})
Formula $C_{16}H_{12}N_4$, Yield 86%, m.p 286°C, R_f value 0.86; IR (KBr, V_{max}, Cm^{-1}): 3048.67 (C-H), 1597.20 (C=C), 1592.88 (C=N)pyridine ring, 1598.97 (N-H), 3049.89 (C-H), 1589.28 (C=C), 1350.71 (C-N indazole ring), 3303.94 (N-H), 3179.08 (C-H), 1600.30 (C=C), 1300.95 (C-H pyrrole ring); ^{1}H NMR (500 MH_Z, $CDCl_3$) δ 5.04 (1H, d, -NH pyrrole ring), 6.12-6.56 (3H, d, t, pyrrole ring), 7.47-8.70 (7H, d, t, m pyridine and aromatic ring), 11.10 (1H, d, -NH indazole ring); MS m/z 260.293.

pyridin-2-yl(5-(2,3,4-trimethoxyphenyl)-2H-1,2,3-triazol-4-yl)methanone (T_1)
Formula $C_{17}H_{16}N_4O_4$, Yield 84%, m.p 285°C, R_f value 0.84; IR (KBr, V_{max}, Cm^{-1}): 3063.94(C-H), 1538.41 (C=C), 1642.66 (C=N) pyridine ring, 1756.79(C=O), 3346.19 (N-H), 1642.94 (C=N), 1100.11 (N-N triazole), 3179.99 (C-H), 2840.42 (C-H), 1550.83 (C=C), 1250.28 (C-O), 1450.63 (C-H trimethoxy benzene); ^{1}H NMR (500 MH_Z, $CDCl_3$) δ 3.83 (9H, S, -OCH_3), 6.12-8.69 (6H, d, t, m pyridine and aromatic ring), 11.58 (1H, S, -NH triazole); MS m/z 340.333.

[5-(4-nitrophenyl)-2*H*-1,2,3-triazol-4-yl](pyridin-2-yl)methanone (T_2)
Formula $C_{14}H_9N_5O_3$, Yield 86%, m.p 286°C, R_f value 0.86; IR (KBr, V_{max}, Cm^{-1}): 3073.85 (C-H), 1590.76 (C=C), 1623.82 (C=N) pyridine ring), 1720.21 (C=O), 3350.56(N-H), 1645.97 (C=N), 980.42 (N-N triazole ring), 1623.75 (C=C), 1300.68 (C-N nitro benzene); ^{1}H NMR (500 MH_Z, $CDCl_3$) δ 7.45-8.66 (8H, d, t, m pyridine and aromatic ring) 11.25 (1H, S, -NH triazole ring); MS m/z 295.252

pyridin-2-yl(5-pyridin-2-yl-2*H*-1,2,3-triazol-4-yl)methanone (T_3)
Formula $C_{13}H_9N_5O$, Yield 86%, m.p 284°C, R_f value 0.86; IR (KBr, V_{max}, Cm^{-1}): 3062.34 (C-H), 1590.89 (C=C), 1642.61 (C=N) pyridine ring, 1759.23 (C=O), 3317.95 (N-H), 1600.70 (C=N), 1000.44 (N-N triazole ring), 3000.87 (C-H), 1590.59 (C=C), 1480.32 (C=N pyridine ring); ^{1}H NMR (500 MH_Z, $CDCl_3$) δ 7.04-9.07 (8H, d, t, m pyridine and aromatic ring) 10.81 (1H, S, -NH triazole ring); MS m/z 251.243

[5-(4-methoxyphenyl)-2*H*-1,2,3-triazol-4-yl](pyridin-2-yl)methanone (T_4)
Formula $C_{16}H_{16}N_4O_4$, Yield 84%, m.p 286°C, R_f value 0.85; IR (KBr, V_{max}, Cm^{-1}): 3062.77 (C-H), 1590.90 (C=C), 1582.28 (C=N) pyridine ring , 1731.66 (C=O), 3300.53 (N-H), 1600.35 (C=N), 1100.80 (N-N triazole ring), 2830.47 (C-H), 1250.63 (C-O methoxy benzene); ^{1}H NMR (500 MH_Z, $CDCl_3$) δ 3.70 (3H, S, -OCH_3), 6.83-8.95 (8H, d, t, m pyridine and aromatic ring), δ 11.37 (1H, S, -NH triazole ring); MS m/z 296.323

(5-(4-hydroxy-3-methoxyphenyl)-2H-1,2,3-triazol-4-yl)(pyridin-2-yl)methanone (T_5)
Formula $C_{15}H_{12}N_4O_3$, Yield 86%, m.p 284°C, R_f value 0.84; IR (KBr, V_{max}, Cm^{-1}): 3021.26 (C-H), 1590.92 (C=C), 1521.74 (C=N pyridine ring), 1762.38 (C=O), 3300.60 (N-H), 1600.99 (C=N), 1110.49 (N-N triazole ring), 3500.72 (O-H), 2830.58 (C-H), 1250.29 (C-O hydroxyl methoxy benzene); ^{1}H NMR (500 MH_Z, $CDCl_3$) δ 3.69 (3H, S, -OCH_3), 5.26 (1H, S, -OH), 6.82-8.78 (7H, d, t, m pyridine and aromatic ring), 10.84 (1H, S, -NH triazole ring); MS m/z 296.280

(5-anthracen-9-yl-2*H*-1,2,3-triazol-4-yl)(pyridin-2-yl)methanone (T_6)
Formula $C_{12}H_{14}N_4O$, Yield 84%, m.p 286°C, R_f value 0.86; IR (KBr, V_{max}, Cm^{-1}): 3021.60 (C-H), 1590.99 (C=C), 1637.49 (C=N) pyridine ring, 1742.72 (C=O), 3356.58 (N-H), 1600.29 (C=N triazole ring), 985.84 (N-N triazole ring), 3100.36 (C-H), 1520.68 (C=C phenanthrene ring); ^{1}H NMR (500 MH_Z, $CDCl_3$) δ 7.29-9.10 (13H, d, t, m pyridine and anthracene ring), 11.29 (1H, S, -NH triazole ring); MS m/z 350.372.

(5-(naphthalen-1-yl)-2H-1,2,3-triazol-4-yl)(pyridin-2-yl)methanone (T_7)
Formula $C_{18}H_{12}N_4O$, Yield 86%, m.p 284°C, R_f value 0.85; IR (KBr, V_{max}, Cm^{-1}): 3072.89(C-H), 1590.51 (C=C), 1596.94 (C=N) pyridine ring, 1763.31 (C=O), 3300.86 (N-H), 1600.40 (C=N), 1021.69 (N-N triazole ring), 3320.73 (N-H), 2900.55 (C-H), 1200.25 (C-N naphthalene ring); ^{1}H NMR (500 MH_Z, $CDCl_3$) δ 7.27-9.12 (11H, d ,t, m pyridine and naphthalene ring), 10.69 (1H, S, -NH triazole ring); MS m/z 300.314
00…..

[5-(piperazin-2-yl)-2*H*-1,2,3-triazol-4-yl](pyridin-2-yl)methanone (T_8)

Formula $C_{12}H_{14}N_6O$, Yield 84%,m.p 286°C, R_f value 0.84; IR (KBr, V_{max}, Cm^{-1}): 3014.45 (C-H), 1590.62 (C=C), 1532.91 (C=N), 1350.39 pyridine ring, 1700.48 (C=O), 3300 (N-H), 1631.76(C=N), 1055.30 (N-N triazole ring), 3319.86 (N-H), 2900.52 (C-H), 1050.67 (C-N piperazine ring); ^{1}H NMR (500 MH_Z, $CDCl_3$) δ 2.24-4.54 (9H, m, piperazine ring), 7.85-8.82 (4H, m, pyridine ring), 11.58 (1H, S, -NH triazole ring); MS m/z 258.279

(5-furan-2-yl-2*H*-1,2,3-triazol-4-yl)(pyridin-2-yl)methanone (T_9)

Formula $C_{12}H_8N_4O_2$, Yield 86%, m.p 284°C, R_f value 0.86; IR (KBr, V_{max}, Cm^{-1}): 3092.93 (C-H), 1590.22 (C=C), 1521.78 (C=N)pyridine ring, 1752.57 (C=O), 3300.33 (N-H), 1627.46 (C=N), 1120.64 (N-N triazole ring), 3100.96 (C-H), 1600.24 (C=C), 1200.43 (C-O furan ring); ^{1}H NMR (500 MH_Z, $CDCl_3$) δ 6.3-7.4 (3H, d, t, oxole ring), 7.73-8.93 (4H, t, m, pyridine ring), 11.44 (1H, S, -NH triazole ring); MS m/z 240.217

Pyridin-2-yl[5-(1*H*-pyrrol-2-yl)-2*H*-1,2,3-triazol-4-yl]methanone (T_{10})

Formula $C_{12}H_9N_5O$, Yield :84%, m.p 286°C, R_f value 0.84; IR (KBr, V_{max}, Cm^{-1}): 3032.71 (C-H), 1590.41 (C=C), 1632.41 (C=N) pyridine ring, 1784.96 (C=O), 3300.27 (N-H), 1645.50 (C=N), 990.96 (N-N triazole ring), 3268.67 (N-H), 3100.37 (C-H), 1600.76 (C=C), 1300.64 (C-N pyrrole ring); ^{1}H NMR (500 MH_Z, $CDCl_3$) δ 5.12-6.68 (4H, d, t, pyrrole ring), 7.77-9.13 (4H, d(2), t(2) pyridine ring), 11.52 (1H, S, -NH triazole ring); MS m/z 239.232.

6'-amino-4'-(3,4,5-trimethoxyphenyl)-2,3'-bipyridine-5'-carbonitrile (P_1)

Formula $C_{20}H_{18}N_4O_3$, Yield 84%, m.p 286°C, R_f value 0.84; IR (KBr, V_{max}, Cm^{-1}): 3082.86 (C-H), 1572.46 (C=C), 1613.74 (C=N) pyridine ring, 3400.24 (N-H), 2240.97 (C≡N), 3100.86 (C-H), 1650.24 (C=N), 1450.86 (C=C amino pyridine ring), 3000.85 (C-H), 2840.47 (C-H), 1550.52 (C=C), 1250.26 (C-O), 1450.85 (C-H trimethoxy ring); ^{1}H NMR (500 MH_Z, $CDCl_3$) δ 3.43 (9H, S, $-OCH_3$), 4.45 (2H, S, $-NH_2$), 6.84-8.69 (6H, t, m pyridine and aromatic ring), 9.44 (1H, S, 2-amino-3-cyano pyridine ring); MS m/z 362.381

6'-amino-4'-(4-nitrophenyl)-2,3'-bipyridine-5'-carbonitrile (P_2)

Formula $C_{17}H_{11}N_5O_2$, Yield 85%, m.p 285°C, R_f value 0.86; IR (KBr, V_{max}, Cm^{-1}): 3012.86 (C-H), 1488.26 (C=C), 1591.76 (C=N), 1350.36 pyridine ring, 3367.85 (N-H), 2246.26(C≡N), 3100.85 (C-H), 1643.97(C=N), 1450.47 (C=C amino pyridine ring), 3050.47 (C-H), 1540.86 (C=C), 1300.77 (C-N nitro benzene); ^{1}H NMR (500 MH_Z, $CDCl_3$) δ 4.22 (2H, S, $-NH_2$), 7.74-8.64 (4H, d(4) nitro benzene and pyridine ring); 9.43 (1H, S, 2-amino-3-cyano pyridine ring); MS m/z 317.301.

6'-amino-2,3':4',3''-terpyridine-5'-carbonitrile (P_3)

Formula $C_{16}H_{11}N_5$, Yield 86%, m.p 284°C, R_f value 0.84; IR (KBr, V_{max}, Cm^{-1}): 3016.25 (C-H), 1481.36 (C=C), 1622.37 (C=N) pyridine ring, 3400.86 (N-H), 2251.35 (C≡N), 3100.85 (C-H), 1623.26 (C=N), 1450.86 (C=C amino pyridine ring), 3000.86 (C-H), 1590.26 (C=C), 1480.26 (C=N pyridine ring); ^{1}H NMR (500 MH_Z, $CDCl_3$) δ 4.38 (2H, S, $-NH_2$), 7.31-8.81 (8H, m, pyridine rings), 9.15 (1H, S, 2-amino-3-cyano pyridine ring); MS m/z 273.292

6'-amino-4'-(4-methoxyphenyl)-2,3'-bipyridine-5'-carbonitrile (P_4)

Formula $C_{18}H_{14}N_4O$, Yield 84%, m.p 286°C, R_f value 0.86; IR (KBr, V_{max}, Cm^{-1}): 3028.36 (C-H), 1561.78 (C=C), 1590.97 (C=N) pyridine ring, 3400.89 (N-H), 2235.75(C≡N), 3100.24 (C-H), 1650.13 (C=N), 1450.67 (C=C aminopyridine ring); 3000.26 (C-H), 2840.47 (C-H), 1550.37 (C=C), 1250.47 (C-0), 1450.18 (C-H methoxy benzene); ^{1}H NMR (500 MH_Z, $CDCl_3$) δ 3.55 (3H, S, $-OCH_3$), 4.20 (2H, S, $-NH_2$), 6.66-8.34 (8H, m, pyridine and aromatic ring), 9.48 (1H, S, 2-amino-3-cyano pyridine ring); MS m/z 302.329

6'-amino-4'-(4-hydroxy-3-methoxyphenyl)-2,3'-bipyridine-5'-carbonitrile (P_5)

Formula $C_{18}H_{14}N_4O_2$, Yield 86%, m.p 284°C, R_f value 0.85; IR (KBr, V_{max}, Cm^{-1}): 3075.36 (C-H), 1466.46 (C=C), 1634.86 (C=N) pyridine ring, 3400.24 (N-H), 2250.64 (C=N), 3160.64 (C-H), 1650.74 (C=N), 1469.65(C=C aminopyridine ring)3200.63 (O-H), 2840.78 (C-H), 1250.63 (C-O), 1450.75 (C-H), 3000.64 (C-H), 1550 .54(C=C hydroxyl methoxy benzene); ^{1}H NMR (500 MH_Z, $CDCl_3$) δ 3.34 (3H, S, $-OCH_3$), 4.15 (2H, S, $-NH_2$), 5.25 (1H, S, -OH), 6.87-7.80 (7H, m, pyridine and aromatic ring), 9.26 (1H, S, 2-amino-3-cyano pyridine ring); MS m/z 318.329

2-amino-4-(anthracen-10-yl)-5-(pyridin-2-yl)nicotinonitrile (P_6)

Formula $C_{25}H_{16}N_4$, Yield 84%, m.p 286°C, R_f value 0.86; IR (KBr, V_{max}, Cm^{-1}): 3075.66 (C-H), 1489.84 (C=C), 1631.26 (C=N) pyridine ring, 3400.85 (N-H), 2258.85 (C≡N), 3154.73 (C-H), 1621.25 (C=N), 1497.75(C=C), 1250.75 aminopyridine ring), 3100.85 (C-H), 1620.36 (C=C phenanthrene ring); ^{1}H NMR (500 MH_Z, $CDCl_3$) δ 4.58 (2H, S, $-NH_2$), 7.22-8.67 (13H, m, pyridine and anthracene ring), 9.10 (1H, S, 2-amino-3-cyano pyridine ring); MS m/z 372.42.

2-amino-4-(naphthalen-1-yl)-5-(pyridin-2-yl)nicotinonitrile (P_7)

Formula $C_{21}H_{14}N_4$, Yield 86%, m.p 285°C, R_f value 0.84; IR (KBr, V_{max}, Cm^{-1}): 3086.76 (C-H), 1592.75 (C=C), 1623.85 (C=N) pyridine ring), 3400.63 (N-H), 2632.76 (C≡N), 3100.64 (C-H), 1650.69 (C=N), 1475.87 (C=C amino pyridine ring), 3300.84 (N-H), 2900.25 (C-H), 1200.37 (C-N piperazine ring); ^{1}H NMR (500 MH_Z, $CDCl_3$) δ 4.44 (2H, S, $-NH_2$), 7.14-8.65 (11H, m, pyridine and naphthalene ring), 9.54 (1H, S, 2-amino-3-cyano-pyridine ring); MS m/z 322.362

2-amino-4-(piperazin-1-yl)-5-(pyridin-2-yl)nicotinonitrile (P_8)

Formula $C_{15}H_{16}N_6$, Yield 84%, m.p 284°C, R_f value 0.86; IR (KBr, V_{max}, Cm^{-1}): 3076.58 (C-H), 1470.57 (C=C), 1597.61 (C=N)pyridine ring, 3400.46 (N-H), 2233.14 (C≡N), 3000.58 (C-H), 1650.68 (C=N), 1447.58 (C=C amino pyridine ring), 3300.47 (N-H), 2900.26(C-H), 1100.64 (C-N piperazine ring); ^{1}H NMR (500 MH_Z, $CDCl_3$) δ 2.26-3.42 (9H, t, m piperazine ring), 4.56 (2H, S, $-NH_2$), 7.20-8.24 (4H, d, t pyridine ring), 9.35 (1H, S, 2-amino-3-cyano pyridine ring); MS m/z 280.327

2-amino-4-(furan-2-yl)-5-(pyridin-2-yl)nicotinonitrile (P_9)

Formula $C_{15}H_{10}N_4O$, Yield 86%, m.p 286°C, R_f value 0.84; IR (KBr, V_{max}, Cm^{-1}): 3075.68 (C-H), 1582.15 (C=C), 1622.65 (C=N)pyridine ring, 3400.54 (N-H), 2212.24 (C≡N), 3100.46 (C-H), 1650.75 (C=N), 1467.25 (C=C amino pyridine ring), 3100.86 (C-H), 1600.90 (C=C), 1220.13(C-O); ^{1}H NMR (500 MHz, $CDCl_3$) δ 4.08 (2H, S, -NH_2), 6.30-6.84 (3H, d, t, furan ring), 7.12-8.42 (4H, m, pyridine ring), 8.95 (1H, S, 2-amino-3-cyano pyridine ring); MS m/z 262.266

2-amino-5-(pyridin-2-yl)-4-(1H-pyrrol-2-yl)nicotinonitrile (P_{10})

Formula $C_{15}H_{11}N_5$, Yield 84%, m.p 286°C, R_f value 0.86; IR (KBr, V_{max}, Cm^{-1}): 3021.57 (C-H), 1498.47 (C=C), 1638.46 (C=N) pyridine ring, 3400.58 (N-H), 2241.58 (C≡N), 3100.86 (C-H), 1650.25 (C=N), 1429.57 (C=C aminopyridine ring), 3400.86 (N-H), 3100.57 (C-H), 1600.74 (C=C), 1300.68 (C-N pyrrole ring); ^{1}H NMR (500 MHz, $CDCl_3$) δ 4.00 (2H, S, -NH_2), 5.05-6.24 (4H, d, t, pyrrole ring), 7.31-8.25 (4H, d, t pyridine ring), 9.05 (1H, S, 2-amino-3-cyano pyridine ring); MS m/z 261.281.

Pyridine-based compounds C_8, I_7, I_8, P_1, and T_3 (which showed higher % inhibition in against TB) distinct fluorescence intensities when exposed to UV illumination (384 nm) depicted in **Figure 4**. The variation in emission brightness reflects differences in molecular structure and electronic environment, highlighting the potential of these derivatives for luminescence-based biological and analytical applications.

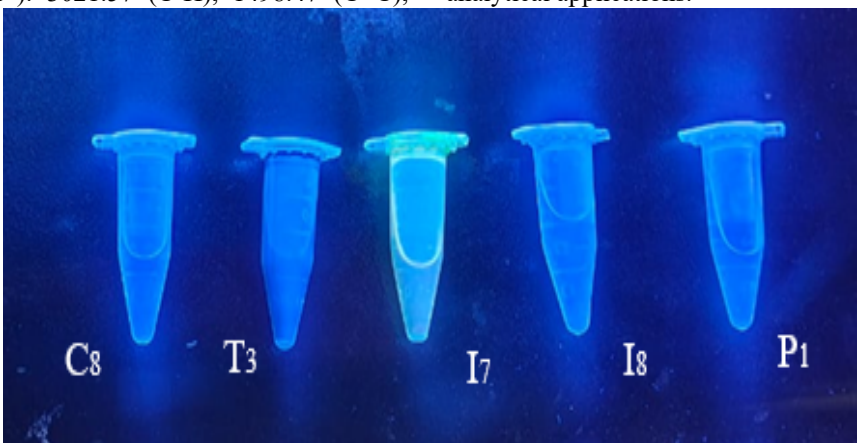

Figure 4. Luminescence of pyridine derivatives under UV light (365 nm

Antitubercular activity by Luciferase reporter assay method

Observations of Luciferase reporter assay which had been performed to evaluate *in vitro* antitubercular activity against drug resistant *M. tuberculosis* H37Rv strain of indicated that several designed compounds exhibit strong inhibitory effects shown in **Table 5**, and **Figure 5**. Compounds such as I_7 (98.82%), P_1 (97.42%), I_8 (97.38%), and C_8 (95.54%), demonstrated excellent activity with greater than 95% inhibition, indicating potent bactericidal potential. Other promising candidates like C_1, C_5, T_2, T_3, T_9, I_1, I_3, I_6, I_{10}, and P_4 also showed high inhibition levels between 85-95%, suggesting robust anti-TB efficacy. Moderate inhibition (around 70–85%) was observed with compounds such as T_1, T_4, T_5, I_4, I_9, and P_5. On the other hand, the remaining molecules showed lower inhibitory activity (below 70%), indicating limited effectiveness. Overall, several compounds outperformed typical activity thresholds, marking them as excellent leads for further development. Particularly, the "I" and "P" series compounds like I_7, I_8, and P_1 emerge as highly promising candidates for future optimization and evaluation.

Table 5. Relative luminescence units (RLU) and percentage inhibition of compounds against Mycobacterium tuberculosis H37Rv.

Compound code	RLU Values	% Inhibition	Compound code	RLU Values	% Inhibition
C_1	53	91.82	T_1	156	74.23
C_2	1165	0.89	T_2	58	90.86
C_3	654	28.58	T_3	48	94.14
C_4	846	19.37	T_4	182	80.83
C_5	65	90.47	T_5	139	78.21

C_6	340	37.43	T_6	228	67.31
C_7	754	32.22	T_7	473	51.24
C_8	46	95.54	T_8	878	18.41
C_9	608	21.33	T_9	92	87.26
C_{10}	561	48.12	T_{10}	263	64.31
I_1	63	91.86	P_1	40	97.42
I_2	978	17.83	P_2	240	63.01
I_3	165	85.43	P_3	346	37.11
I_4	180	81.24	P_4	86	88.93
I_5	245	28.23	P_5	186	81.36
I_6	87	88.91	P_6	686	24.21
I_7	24	98.82	P_7	492	53.33
I_8	39	97.38	P_8	983	16.34
I_9	136	78.36	P_9	340	37.42
I_{10}	64	90.52	P_{10}	1045	9.21

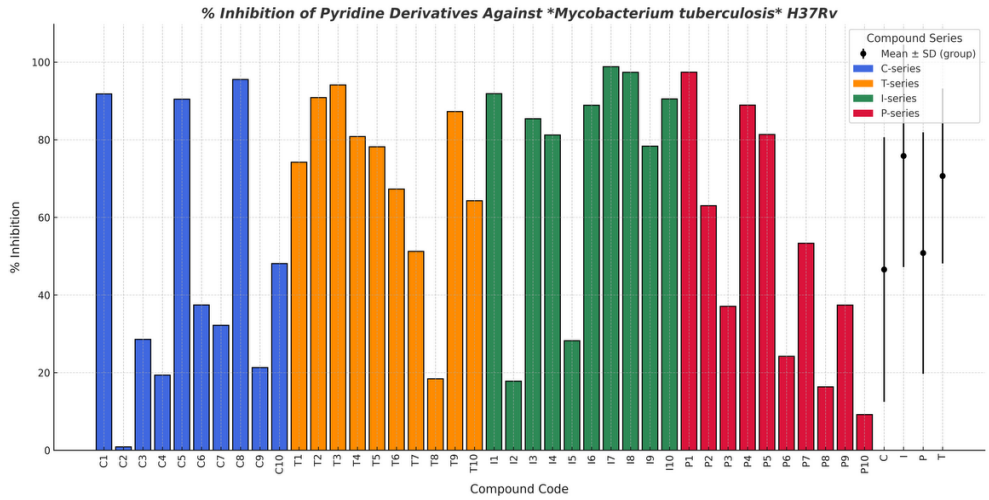

Figure 5. % inhibition of pyridine derivatives against *Mycobacterium tuberculosis* H37Rv

Structure–Activity Relationship (SAR) with RLU–Activity–Luminescence Correlation

The SAR analysis of the synthesized indazolopyridine, cyanopyridine, triazolopyridine, and chalcone derivatives against *Mycobacterium tuberculosis* H37Rv revealed a clear correlation between their RLU values, % inhibition, molecular features, and predicted luminescence. Compounds exhibiting low RLU values demonstrated high inhibition, confirming efficient antimycobacterial action. Among the indazolopyridines, naphthalene derivative I_7 (RLU = 24, 98.82%) and piperazine derivative I_8 (39, 97.38%) showed superior activity, attributed to their rigid fused aromatic systems and electron-donating substituents, which favor π–π interactions, intramolecular charge transfer (ICT), and bright blue-green luminescence. The nitro derivative I_2 (978, 17.83%) displayed reduced activity due to fluorescence quenching and weak target interaction. In the cyanopyridine series, 3,4,5-trimethoxy substituted derivative P_1 (40, 97.42%) exhibited strong donor–acceptor (D–A) characteristics conducive to both ICT fluorescence and enzyme binding. Triazolopyridines T_3 (48, 94.14%) and T_2 (58, 90.86%) were potent due to their conjugated heteroaromatic donors that stabilize π–π* transitions, whereas T_8 (878, 18.41%) lost activity through photoinduced electron transfer (PET). Chalcones C_8 (46, 95.54%) and C_1 (53, 91.82%) displayed strong inhibition and enhanced luminescence owing to α,β-unsaturated conjugation and donor-rich substituents.

Overall, the compounds with high conjugation, planarity, and donor–acceptor balance exhibited both strong antimycobacterial potency and predicted luminescent properties. The integrated docking and QSAR data supported these findings, establishing that molecular

features governing charge delocalization and fluorescence also enhance target affinity, indicating the potential of these scaffolds as theranostic agents combining bioactivity with optical traceability.

Conclusion

In this study, an integrated computational and experimental approach was employed to evaluate the anti-tubercular potential of novel cyanopyridine, triazole, indazole, and chalcone derivatives derived from 2-acetyl pyridinyl prop-2-en-1-one. Molecular docking studies against the DprE1 enzyme revealed several compounds, including T_1, T_5, C_1, I_7, and I_8, with strong binding affinities and favorable interactions with key active site residues, suggesting their potential to inhibit enzymatic activity effectively. The predicted biological activity using the MLR-based QSAR model corroborated these findings, highlighting the same compounds as highly potent inhibitors. ADME profiling further indicated that most of the promising compounds possess favorable pharmacokinetic properties, including high gastrointestinal absorption, drug-likeness, and synthetic accessibility, which support their suitability for further development. Importantly, a clear inverse correlation between RLU values and % inhibition was observed across all series, affirming that efficient inhibitors suppress luminescence from the reporter phage *in vitro* anti-TB assay against *M. tuberculosis* H37Rv. Collectively, these results identify a subset of molecules with a balanced profile of potency, bioavailability, and structural novelty, making them strong candidates for lead optimization. The study underscores the value of combining *in silico* modeling with experimental validation to accelerate anti-TB drug discovery and offers promising scaffolds for the development of novel therapeutics against multidrug-resistant and extensively drug-resistant tuberculosis.

Acknowledgement

We are thankful to DST-FIST laboratory and DST SERB facility of Raghavendra Institute of Pharmaceutical Education and Research (RIPER) – Autonomous, Ananthapuramu for the support of synthesis and molecular docking studies. We also thank to Dr. Y. Padmanabha Reddy, Principal, RIPER for providing facilities to carry out this research work.

Confliction of Interest

The authors expressed no conflict of interest.

REFERENCE

[1] S.-X. Zhang, F.-Y. Miao, J. Yang, W.-T. Zhou, S. Lv, F.-N. Wei, Y. Wang, X.-J. Hu, P. Yin, P.-Y. Zheng, M. Yang, M.-T. Wang, X.-Y. Feng, L. Duan, G.-B. Yang, J.-C. Wang, Z.-H. Lu, Global, regional, and national burden of HIV-negative tuberculosis, 1990–2021: findings from the Global Burden of Disease Study 2021, Infectious Diseases of Poverty 13 (2024) 60. https://doi.org/10.1186/s40249-024-01227-y.

[2] H. Mezgebe, T. Gebrecherkos, D. Hagos, S. Muthupandian, Prevalence of Smear-Positive, Rifampicin-Resistant Mycobacterium tuberculosis and Related Factors Among Residents with Cough in Northern Ethiopian Refugee Health Facilities, Infection and Drug Resistance Volume 17 (2024) 1135–1145. https://doi.org/10.2147/IDR.S453306.

[3] C.M. Stein, Post-pandemic tuberculosis incidence: potential success of active case finding?, Thorax 79 (2024) 299–300. https://doi.org/10.1136/thorax-2023-221224.

[4] K.J. Seung, S. Keshavjee, M.L. Rich, Multidrug-Resistant Tuberculosis and Extensively Drug-Resistant Tuberculosis, Cold Spring Harbor Perspectives in Medicine 5 (2015) a017863. https://doi.org/10.1101/cshperspect.a017863.

[5] R. Jubilee, M. Komala, S. Patel, Therapeutic Potential of Resveratrol and Lignans in the Management of Tuberculosis, Cell Biochemistry and Biophysics 82 (2024) 1809–1823. https://doi.org/10.1007/s12013-024-01378-7.

[6] R. Mazumder, Ichudaule, A. Ghosh, S. Deb, R. Ghosh, Significance of Chalcone Scaffolds in Medicinal Chemistry, Top Curr Chem 382 (2024) 22. https://doi.org/10.1007/s41061-024-00468-7.

[7] S.K. Raju, P. Sekar, M. Sankarganesh, M. Murphy, Design, synthesis, characterization and computational studies of chalcone-imines as potent anti-breast cancer agents, J Mol Struct 1342 (2025) 142672. https://doi.org/10.1016/j.molstruc.2025.142672.

[8] Praveen Sekar, Shridharshini Kumar, Senthil Kumar Raju, Chemistry and synthetic methodologies of chalcones and their derivatives: A review, International Journal of Biological and Pharmaceutical Sciences Archive 5 (2023) 051–072. https://doi.org/10.53771/ijbpsa.2023.5.1.0020.

[9] D. L. S., K. M. K., G. Thamilselvan, Design, synthesis and anti-Tb evaluation of chalcone derivatives as novel inhibitors of InhA, J Biomol Struct Dyn 41 (2023) 15165–15176. https://doi.org/10.1080/07391102.2023.2227711.

[10] B. Anagani, J. Singh, J.P. Bassin, G.S. Besra, C. Benham, T.R.K. Reddy, J.A.G. Cox, M. Goyal, Identification and validation of the mode of action of the chalcone anti-mycobacterial compounds, The Cell Surface 6 (2020) 100041. https://doi.org/10.1016/j.tcsw.2020.100041.

[11] H. Tavanoji, G. Latambale, K. Juvale, A comprehensive review on indole-chalcone hybrid as promising scaffold with diverse therapeutic potential, Bioorg Med Chem 131 (2025) 118391. https://doi.org/10.1016/j.bmc.2025.118391.

[12] R. Baptista, S. Bhowmick, J. Shen, L.A.J. Mur, Molecular Docking Suggests the Targets of Anti-Mycobacterial Natural Products, Molecules 26 (2021) 475. https://doi.org/10.3390/molecules26020475.

[13] E. Schroeder, O. de Souza, D. Santos, J. Blanchard, L. Basso, Drugs that Inhibit Mycolic Acid Biosynthesis in Mycobacterium tuberculosis, Curr Pharm Biotechnol 3 (2002) 197–225. https://doi.org/10.2174/1389201023378328.

[14] A. Shetty, T. Dick, Mycobacterial Cell Wall Synthesis Inhibitors Cause Lethal ATP Burst, Front Microbiol 9 (2018). https://doi.org/10.3389/fmicb.2018.01898.

[15] C. Lu, C. Wu, D. Ghoreishi, W. Chen, L. Wang, W.

Damm, G. A. Ross, M. K. Dahlgren, E. Russell, C. D. Von Bargen, R. Abel, R. A. Friesner, E. D. Harder, OPLS4: Improving Force Field Accuracy on Challenging Regimes of Chemical Space, Journal of Chemical Theory and Computation 17 (2021) 4291–4300. https://doi.org/10.1021/acs.jctc.1c00302.

[16] B.K. Kumar, Faheem, K.V.G.C. Sekhar, R. Ojha, V.K. Prajapati, A. Pai, S. Murugesan, Pharmacophore based virtual screening, molecular docking, molecular dynamics and MM-GBSA approach for identification of prospective SARS-CoV-2 inhibitor from natural product databases, J Biomol Struct Dyn 0 (2020) 1–24. https://doi.org/10.1080/07391102.2020.1824814.

[17] G. Madhavi Sastry, M. Adzhigirey, T. Day, R. Annabhimoju, W. Sherman, Protein and ligand preparation: Parameters, protocols, and influence on virtual screening enrichments, Journal of Computer-Aided Molecular Design 27 (2013) 221–234. https://doi.org/10.1007/s10822-013-9644-8.

[18] Y.-Y. Cheng, H. Yuan, Quantitative study of electrostatic and steric effects on physicochemical property and biological activity, Journal of Molecular Graphics and Modelling 24 (2006) 219–226. https://doi.org/10.1016/j.jmgm.2005.08.005.

[19] N.A.A. Elkanzi, H. Hrichi, R.A. Alolayan, W. Derafa, F.M. Zahou, R.B. Bakr, Synthesis of Chalcones Derivatives and Their Biological Activities: A Review, ACS Omega 7 (2022) 27769–27786. https://doi.org/10.1021/acsomega.2c01779.

[20] A. Kumar, S. Sharma, V.D. Tripathi, S. Srivastava, Synthesis of chalcones and flavanones using Julia–Kocienski olefination, Tetrahedron 66 (2010) 9445–9449. https://doi.org/10.1016/j.tet.2010.09.089.

[21] J.H. Tomma, S.F. Abbas, A.H. Al-Dujaili, New Quinolin-2-one, Indazole, and Benzisoxazole Derivatives Derived from Chalcones: Synthesis, Characterization, and Biological Activity, Russian Journal of Organic Chemistry 59 (2023) 1027–1032. https://doi.org/10.1134/S107042802306009X.

[22] A. Sharma, A. Saraswat, Overview on cumulative synthetic approaches for chalcone based functionalized scaffolds, Journal of the Indian Chemical Society 98 (2021) 100028. https://doi.org/10.1016/j.jics.2021.100028.

[23] M. Raghavender, A.K. Kumar, V. Sunitha, T. Vishnu, P. Jalapathi, Synthesis and Cytotoxicity of Chalcone Based 1,2,3-Triazole Derivatives, Russian Journal of General Chemistry 90 (2020) 697–702. https://doi.org/10.1134/S1070363220040210.

[24] S.E. Beutick, P. Vermeeren, T.A. Hamlin, The 1,3-Dipolar Cycloaddition: From Conception to Quantum Chemical Design, Chemistry – An Asian Journal 17 (2022). https://doi.org/10.1002/asia.202200553.

[25] N. Kumar, A. Chauhan, S. Drabu, Synthesis of cyanopyridine and pyrimidine analogues as new anti-inflammatory and antimicrobial agents, Biomedicine & Pharmacotherapy 65 (2011) 375–380. https://doi.org/10.1016/j.biopha.2011.04.023.

[26] P. Chitale, A.D. Lemenze, E.C. Fogarty, A. Shah, C. Grady, A.R. Odom-Mabey, W.E. Johnson, J.H. Yang, A.M. Eren, R. Brosch, P. Kumar, D. Alland, A comprehensive update to the Mycobacterium tuberculosis H37Rv reference genome, Nature Communications 13 (2022) 7068. https://doi.org/10.1038/s41467-022-34853-x.

[27] A. Daina, O. Michielin, V. Zoete, SwissADME: a free web tool to evaluate pharmacokinetics, drug-likeness and medicinal chemistry friendliness of small molecules, Scientific Reports 7 (2017) 42717. https://doi.org/10.1038/srep42717